Winglet Design for a Fairchild Merlin III using CFD Analysis

Kai Lehmkuehler[1], Dr KC Wong[2]

[1] *Research Student, School of Aerospace, Mechanical and Mechatronic Engineering, The University of Sydney*
[2] *Senior Lecturer, School of Aerospace, Mechanical and Mechatronic Engineering, The University of Sydney*

Abstract

This paper investigates the aerodynamic characteristics of a winglet design for a Fairchild Merlin III 8-seat, twin turboprop aircraft. The winglet was designed by the aircraft owner to improve the aesthetics of the aeroplane. To ensure that the winglet will not have any negative effect on the aircraft, a series of comparative CFD simulations was carried out. Confidence in the results was gained by comparison with accepted computational and empirical methods. Good agreement was achieved. The solutions were found to be mesh dependent due to hardware restrictions, but converging with decreasing mesh size. The results for the winglet showed a maximum 1.3% increase in L/D of the wing. A strong leading edge vortex created by the high sweep of the winglet severely limited the performance gains. Based on the findings for the original winglet, a new, improved design was tested. It featured less sweep and twice the surface area, with a NACA 6-series aerofoil. This new design improved the cruise L/D of the wing by 5%, which is a threefold improvement over the original winglet. At the same time, the skin friction drag was found to be similar, despite the large increase in area.

Introduction

This paper contains work which was done in partial requirement for the first author's honours thesis [1]. The aim of this project was to investigate the aerodynamic properties of a winglet design and to develop an improved version if necessary. The aircraft of concern in this project was a Fairchild Merlin 3, a twin turboprop executive transport. The original Hoerner wing tip and the initial winglet designed by the aircraft owner to improve the aesthetics of the aeroplane are shown in Figure 1. Dimensions of the winglet are given in Table 2.

Winglets are small, near vertical lifting surfaces mounted on the wing tips. If carefully designed, they reduce the induced drag of the wing and therefore increase the performance either in terms of less fuel consumption or longer range. Other performance parameters such as

Figure 1: Hoerner tip geometry on the aircraft and original winglet prototype

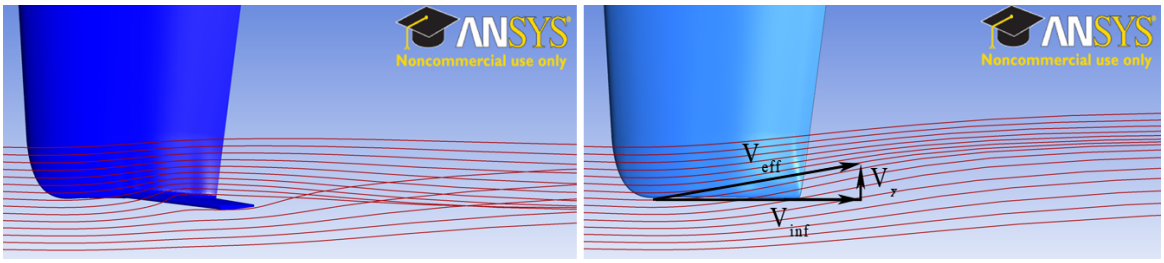

Figure 2: Velocities on wingtip projected in the XY-plane (L) with winglet, (R) without winglet

the rate of climb are also positively affected. The addition of the winglet always adds structural weight. This increase has to be overcompensated by the drag reduction to be viable.

Apart from the possible performance gains winglets are often used for aesthetic reasons. These swept surfaces at the wing tip simply look attractive on an aeroplane. Many business jets use winglets for that reason even on new designs, even though it can be shown that on new wing designs a planar extension of identical surface area and perimeter length is more effective [2].

Winglets alter the pressure field at the wing tip. To do that, they have to produce a significant inboard force normal to the winglet [3], which is illustrated in Figure 2. In the vector diagram it can be seen that the developing wing tip vortex creates an effective angle of attack for a vertical surface parallel to the wing tip. A winglet placed in this flow as shown in the left part of the figure will create a normal force in the Y direction in the same manner as the wing itself creates lift [4]. This side force reduces the lift induced inflow above the wing tip, which can be seen on the left of Figure 2. Comparing the streamlines, the flow inboard of the tip is straightened in Y-direction by the presence of the winglet. The spanwise velocity components (V_y) in the core of the vortex flow around the tips, which contain the highest energy, are substantially reduced. At the same time the tip of the winglet itself creates a new, smaller vortex. Therefore Whitcomb [3] calls winglets 'vortex diffusors', as they spread the tip vortices over a larger area and reduce their energy losses by that process.

Experiment Setup

There are two important flight conditions for the evaluation of winglets. The first is the cruise condition where minimum drag is desired. The second is the landing (or take off) condition where high lift coefficients and possible sideslip may cause unwanted flow separation on the winglet. Using the aircraft flight manual, the following data was calculated: $C_{L,\text{cruise}} = 0.41$ with an angle of attack is about 3 degrees; $C_{L,\text{land}} = 0.99$ and a required angle of attack of $\alpha = 6^\circ$ with full flaps. The aerodynamic properties of the winglet were simulated at those angles of attack.

The general solution method in ANSYS CFX 5 was chosen to be a steady state, incompressible flow and fully turbulent solution. The SST turbulence model was used exclusively. A turbulence intensity of $I = 0.1\%$ was used as the aircraft was assumed to fly into a still atmosphere. Every new simulation was initialised with the closest converged solution available. This method reduced the run time by a third (from 12 to 8 hours). The maximum solvable size was about 6.6 million cells with 8 Gb of computer memory.

To keep the mesh size within reasonable bounds, only the isolated wing of the Merlin III could be analysed. The largest model size possible was 1/10th scale. To maximise the available Reynolds number the simulation flight condition was chosen to be a combination of cruise and landing. The speed used is 125m/s at standard sea level conditions. This equals M=0.36 and the resulting Reynold's number based on the mean aerodynamic chord (MAC) is 1.58 million.

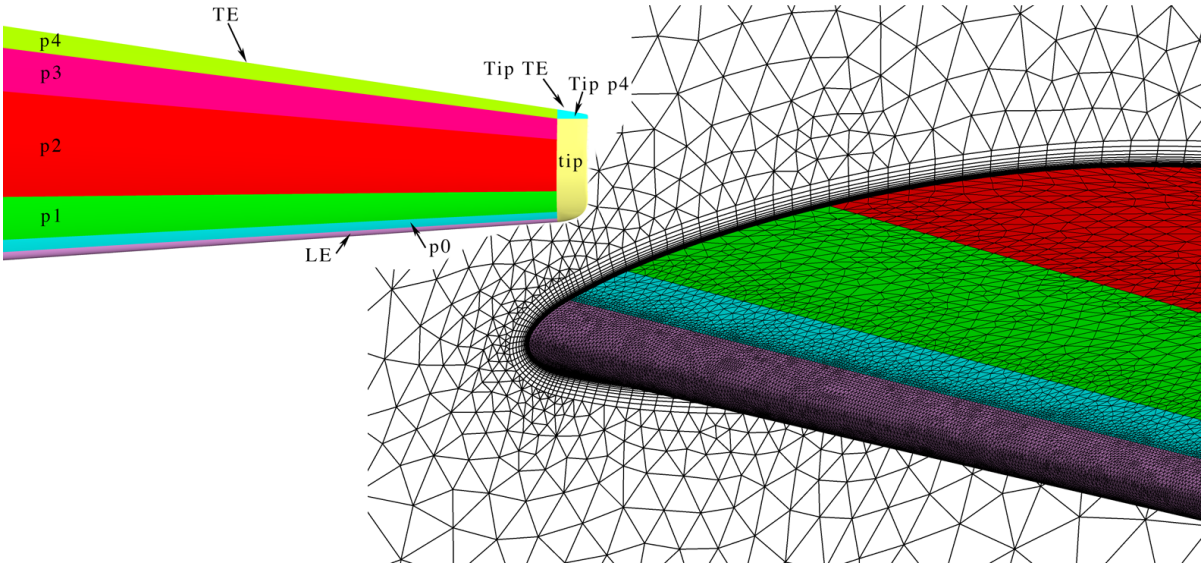

Figure 3: Mesh regions and overview at the symmetry plane

The local Reynolds number on the winglet at these conditions is ≈ 330000, based on its mean aerodynamic chord.

A hybrid mesh, consisting of an unstructured surface- and volume mesh and a structured boundary layer mesh was used. This technique is widely used in the CFD community, although the change in mesh topology introduces uncertainties that are hard to quantify [5].

The surface mesh uses triangular elements that can easily represent complicated surface geometries. This surface mesh was generated first before the boundary layer mesh, which uses hexahedral (prism) elements to create very thin copies of the surface triangles into space away from the surface. This is often referred to as inflation, which results in elements with a very high aspect ratio being very long and thin. This allows cells near the surface without excessive surface mesh sizes. The remaining volume is filled with an unstructured mesh using tetrahedral elements. These start from the surface triangles of the inflation layers up to the domain walls. Figure 3 shows an overview of the mesh near the wing root.

The triangular surface mesh is the basis for the volume mesh and was created first. It determines the resolution of the surface features like leading edge curvature. The size of the surface mesh is defining the final mesh size, so it has to be carefully designed to fit the hardware constraints. The wing was divided in several sections as shown in Figure 3 to adjust the mesh sizes. The meshing guidelines [6] call for a mesh size of 0.1% local chord at the leading- and trailing edge. Due to the limited memory, this had to be eased to 0.5% of the MAC for this project.

The boundary layer mesh contains about 60% of all cells in the mesh. It was designed using some approximations to convert a y^+ value into the required spacing of the first layer off the walls and to determine the boundary layer thickness δ [7]. These yield with the data for the 1/10th scale model:

$$\Delta y = L\,\Delta y^+ \sqrt{74}\,Re_L^{-\frac{13}{14}} = 2.68 \times 10^{-6}\,\mathrm{m} \tag{1}$$

$$\delta = 0.035\,L\,Re_L^{-1/7} = 8.2 \times 10^{-4}\,\mathrm{m} \tag{2}$$

where L is the characteristic length of the flow (here the MAC) and Re_L the simulation Reynolds number based on L. The value for y^+ was restricted to 3 as the requirement of $y^+ \leq 1$ was not possible. Most researchers use advanced meshing methods that include spanwise stretching of the mesh to reduce the resolution perpendicular to the flow [8] and use the gained memory capacity for achieving the $y^+ \leq 1$ requirement.

Table 1: Mesh data

Model	Elements	Tetra	Pyramids	Prisms
Hoerner	5,595,730	2,223,658	-	3,372,072
Winglet	6,086,969	2,428,505	1,928	3,656,536
New Winglet	6,291,584	2,481,580	-	3,810,004

The y^+ value is dependent on the local flow properties, so it can only be determined from the final solution. In this case, most regions on the wing had a y^+ value of 3 or below as specified. The approximation worked well. Near the leading edges, where the local velocity is very high (especially on the winglet), the y^+ values are between 3 and 5.7. This appears to be a good compromise, as the parameters for the inflation layers could only be set globally. Table 1 lists the final mesh sizes for the different cases.

Verification of the CFD Simulation

Due to limited resources, the simulation could not be verified against another viscous solution. Therefore, parts of the results were compared with potential flow methods and empirical data. Good agreement was obtained in all cases.

Firstly, on the symmetry plane (wing root) the flow is nearly two dimensional, as the wing is simulated in isolation. Thus, it is possible to compare the pressure distribution on the wing-symmetry plane intersection to a solution of a 2-d inviscid panel method for aerofoils. The software JAVAfoil [9] was used for this purpose. To find the correct local angle of attack for the 2-D solution, the standard lifting line theory was used with the data for C_L from the CFD solution and the Oswald efficiency e approximated from the same results by fitting a line through the plot C_D vs. C_L^2. The results for $\alpha_{2d} = 3.14°$ are plotted in Figure 4.

In Figure 4(a), it can be seen that the CFD solution matches the inviscid solution accurately in regions, where the boundary layer is thin. In the back of the top half of the viscous case, from about half chord, the thickening boundary layer forms a virtual barrier for the flow and 'changes' the shape of the aerofoil. This is shown in Figure 4(b), where the black line is an iso-contour of $V = 100\,\mathrm{m/s}$. This is the main reason for the differences between the results in this region. For increased accuracy, one would have to analyse this iso-contour in the potential flow method.

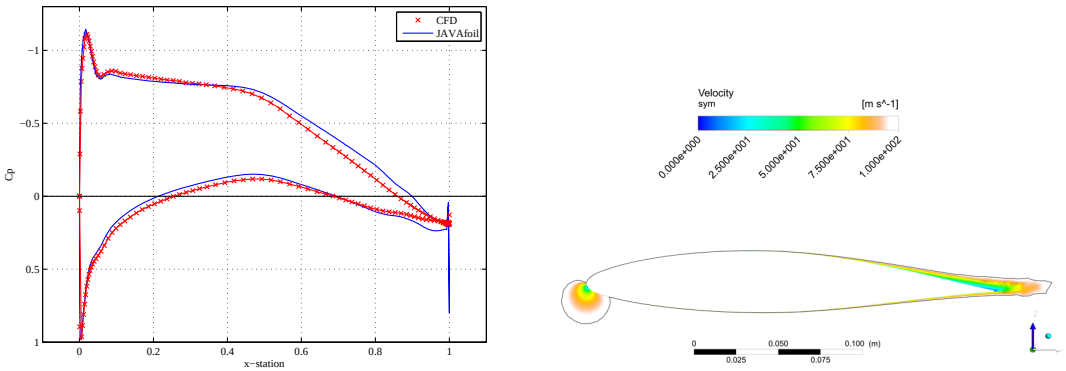

(a) *JAVAfoil pressure distribution compared to CFD data at the wing root*

(b) *Aerofoil shape change due to boundary layer*

Figure 4: CFD vs. JAVAfoil solution

The fully turbulent CFD solution has an almost constant coefficient of friction, C_f, for low angles of attack. The drag due to friction is created in the boundary layer which does not change significantly at these small angles of attack. This changes as α increases beyond 6 degrees. From here on the skin friction drag decreases steadily. This is due to the beginning separation near the trailing edge.

To verify the magnitude of the skin friction drag, Hoerner [10] presents a semi-empirical equation to estimate the skin friction drag of a fully turbulent flow over a flat plate:

$$C_f = 2 \times \frac{0.427}{(\log Re_c - 0.407)^{2.64}} = 0.00828 \tag{3}$$

The factor of two accounts for the two sides of the wing. Taking the mean over a range of angles of attack yields $C_f = 0.00817$. This is an excellent agreement with a difference of about one drag count. During the AIAA drag prediction workshop the variations in drag prediction due to mesh dependency and solver settings were actually larger than the error between the two empirical methods [6].

Next, a 3D potential flow solution was used for the entire wing. The lift curve and the drag polar for the TORNADO [11] solution versus the CFD results are shown in Figure 5(a) and 5(b), respectively. The lift curve agrees well with the CFD results below $\alpha = 6°$. Above $\alpha = 6°$ the effects of viscosity and beginning flow separation starts to influence the CFD solution, which shows a reduction in slope.

The drag polars are of similar shape, especially at low angles of attack. The offset is caused by the profile drag C_{D0}, which is not included into the potential flow results.

One of the most important parameters for any CFD solution is the size of the computational mesh. The finer the mesh, the better the resolution of the flow physics. On the other hand, the available hardware dictates the maximum mesh size. The influence of the mesh on the solution is usually determined by doubling the mesh size at least twice and comparing the results using the Richardson extrapolation [12] or more advanced methods [13].

For this project, it was not possible to increase the mesh size by a factor of two since the working mesh was already near the capacity of the available computer. It was also not possible to half the mesh size, as the solution would not converge on such a coarse mesh. To get an idea of the solution sensitivity on the mesh size, a series of small changes was prepared for comparison with the working mesh. The parameter used for these changes was the mesh expansion ratio.

The expansion ratio was varied between 1.21 and 1.29, which yielded mesh sizes from 6.5 to 5.0 million cells. The first observation during the runs was a slower convergence corresponding

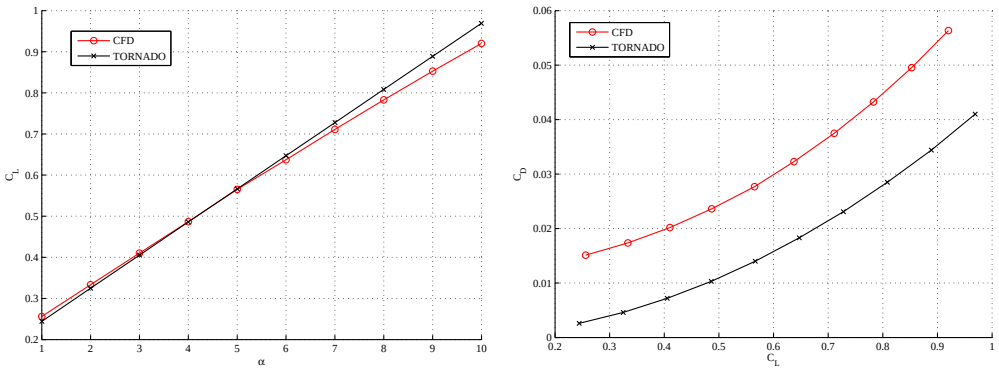

(a) (b)

Figure 5: CFD solution vs. Tornado results for C_L and C_{Di} of the square wingtip

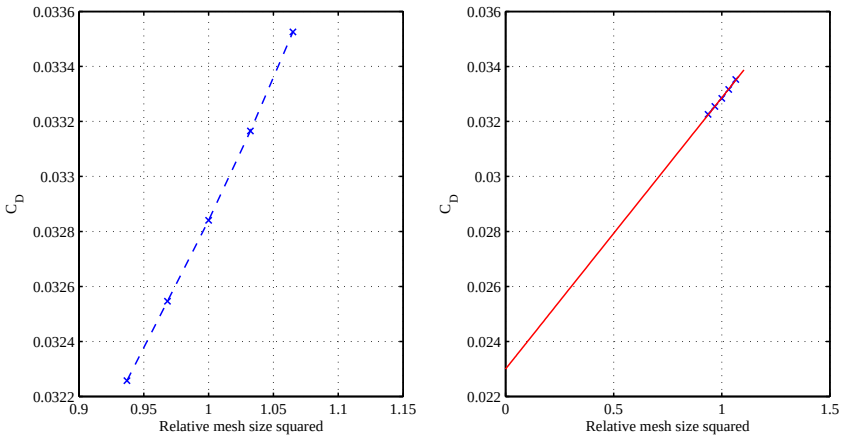

Figure 6: Drag vs. relative meshsize squared

to a diverging grid size diverged from the standard mesh. This was most likely caused by the non optimal interface between the boundary layer mesh and the tetrahedral volume mesh, which was optimized for the 1.25 expansion ratio and is sensitive to disturbances.

The results for the drag coefficient are shown in Figures 6. The left graphs show the results of the computations plotted against the square of the relative mesh size. As second order discretisation schemes were used, the results should change monotonically with grid size inside the asymptotic region. This line can then be extrapolated to yield the result for an infinitesimally small mesh.

Inspecting the graph, the plot shows a linear trend with some disturbances. This indicates convergence with mesh size and most likely the beginning of the asymptotic region. This is supported by the results of the AIAA drag workshops, where the current grid size is just the coarsest size used [6]. In these papers, solutions reach the asymptotic convergence region at about 8 million nodes and above for the transonic flow, which is a more severe case.

Now we can extrapolate the line as shown in the right plots of Figure 6 to an infinitely small mesh size. This results in predictions of $C_D = 0.023$. This drag result is then much closer to the TORNADO prediction of $C_D = 0.0183 + 0.0082 = 0.0265$, if the viscous component of drag is added to the potential flow solution. From this, it appears that in the current solution the drag is over-predicted by substantial amounts.

The size of the computational domain had no appreciable effect on the results. Several sizes were tested and no dependency could be found.

An attempt to run a simulation at $\alpha = 3°$ with the $k-\epsilon$ turbulence model was made to study the effect of the turbulence model on the solution. This attempt failed. The solver terminated after 29 iterations due to a divergence in the solution. Therefore, it appears that the $k-\epsilon$ model is not only less accurate [14], but also introduces numerical instability into the current solution. The decision to use the SST model exclusively was justified by this test. If the SST would not have been available, the entire project would most likely have failed within the hardware restrictions.

The choice of the advection schemes in the CFD solution has a large influence on the final results. Initially, first order schemes were used in the early stages of the mesh development to promote convergence. A major point of concern during this stage were unrealistic drag values. Later in the project the mesh achieved a quality that allowed the use of second order schemes. Immediately, the drag problems disappeared. To quantify the difference in results between the two methods, a comparison was made on the final mesh. The differences in lift are much less significant than the errors for the drag. Overall there is a factor of two between the two

resulting values for the L/D. This impressive difference shows clearly, that for aerodynamic calculations, where the drag is important, the use of second order advection schemes is of paramount importance.

Results and Design Improvement

Due to space restrictions, only the most important findings can be presented in this paper. These will be directly compared between the two winglet designs. For more details refer to [1].

Table 2: Winglet data (Original: left, New: right)

Section:	Flat plate	NACA 64009	Cant angle:	10°	15°
Root chord:	530 mm	540 mm	Root toe angle:	0°	0°
Tip chord:	180 mm	200 mm	Tip toe angle:	−3°	0°
Span:	450 mm	650 mm	Leading edge sweep Λ:	59°	29.5°
Area:	0.14 m^2	0.25 m^2	Taper ratio λ:	0.34	0.335
Aspect ratio:	1.4	1.75	MAC:	383.8 mm	390 mm

Table 2 shows the dimensions of the original winglet. The most critical feature is the leading edge sweep of 59°. This causes the winglet to behave like a delta wing with a very strong leading edge vortex. This is shown in Figures 9(a) and 9(c). The blunt leading edge and the missing aerofoil section adds flow separation near the leading edge. The result is a very inefficient lifting surface with very high surface shear, that leads to high friction drag as shown in Figure 9(b). Figure 8 and Table 3 compare the original winglet with the standard Hoerner wingtip. The improvement in L/D is a small 1.37%, well within the uncertainty of the analysis method. There was no significant change to the stalling characteristics of the wing, even with high sideslip cases. This is discussed in detail in [1].

Clearly, a better solution must be possible, so a new winglet was designed. Several shapes were tested and the final result is described in Table 2. The leading edge sweep was reduced to 30 degrees, a NACA 64009 section was used and the area of the winglet was doubled. A comparison is shown in Figure 7.

The flow fields around the two winglets are compared in Figure 9. Figures 9(a) and 9(d) contain exactly the same streamline source which produces very different flow patterns. The

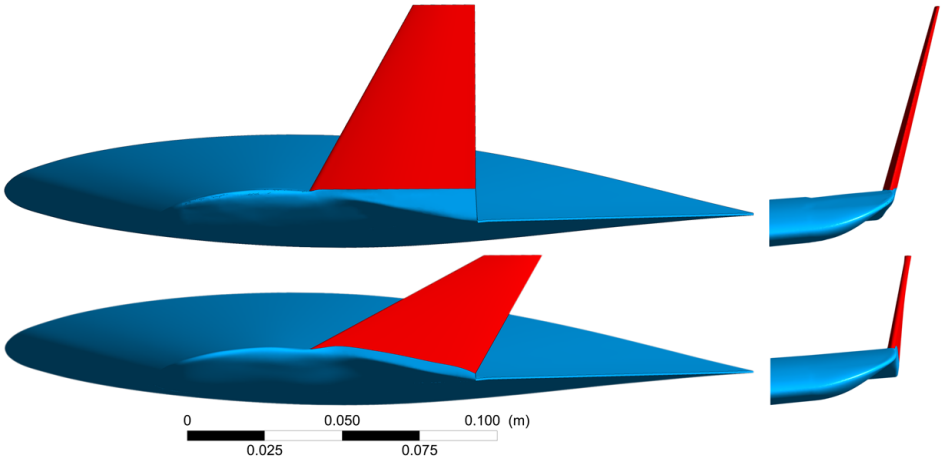

Figure 7: New winglet design (top) and original shape (bottom) (Model 1/10th scale)

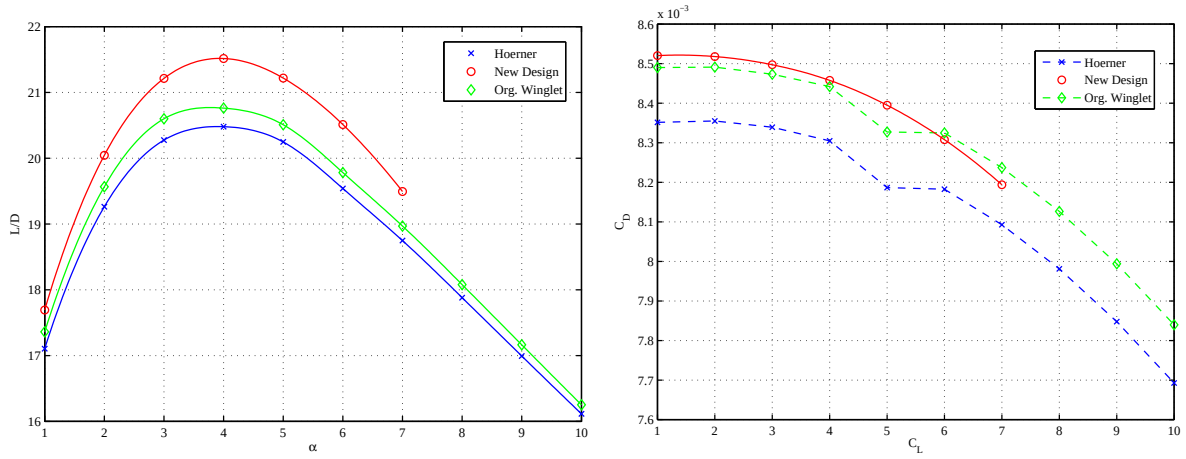

(a) L/D (b) Viscous drag coefficient

Figure 8: Performance comparison of the three wingtips investigated

Table 3: Wing tip performance comparison for the 1/10th scale model (Changes are relative to Hoerner wing tip)

Tip	Area	L/D_{max}	Change	Root BM	Change
Hoerner	-	20.48	-	143.83 Nm	-
Original Wlet	$\approx 0.14\,\mathrm{m}^2$	20.76	1.37%	150.98 Nm	4.97%
New Winglet	$\approx 0.25\,\mathrm{m}^2$	21.52	5.08%	153.37 Nm	6.63%

original winglet created a strong spanwise flow, deflecting the streamlines upwards on both sides and forming the dominating leading edge vortex. In contrast, the new winglet shows only a small vortex, which is generated at the edge of the wing-winglet joint and otherwise no significant vertical flow deflections. The reduction in sweep clearly worked as intended. In Figure 9(f) we can see that the full span of the winglet is active, with a tip vortex produced right at the outer edge. On the original winglet in Figure 9(c), significant parts of the outer span were stalled in the vicinity of the leading edge vortex. Figure 9(f) also shows the junction vortex caused by the non-blended junction. This junction vortex appears to be more defined for the new design in Figure 9(f), as compared to Figure 9(c).

The new winglet geometry generates a significant performance improvement. Table 3 and Figure 8 show a more than threefold increase in maximum L/D at $\alpha = 4°$, while the bending moment at the wing root grows by only 1.5%. Most interestingly, the viscous drag for the new winglet is only slightly higher than the original winglet, despite almost twice the surface area. This is due to the clean flow without any strong sources of surface shear as shown in Figure 9(e).

These results compare well with literature [15][4][16], where the designs achieve gains in L/D of 10% using winglets about twice the size ($0.47\,\mathrm{m}^2$[4] vs. $\approx 0.25\,\mathrm{m}^2$ for this project). Therefore, the efficiency of the new winglet design is in line with the industry standard. The area of the winglet has been kept smaller to honour the initial design intentions of a purely aesthetic improvement. The non-optimal wing-winglet juncture has room for improvement.

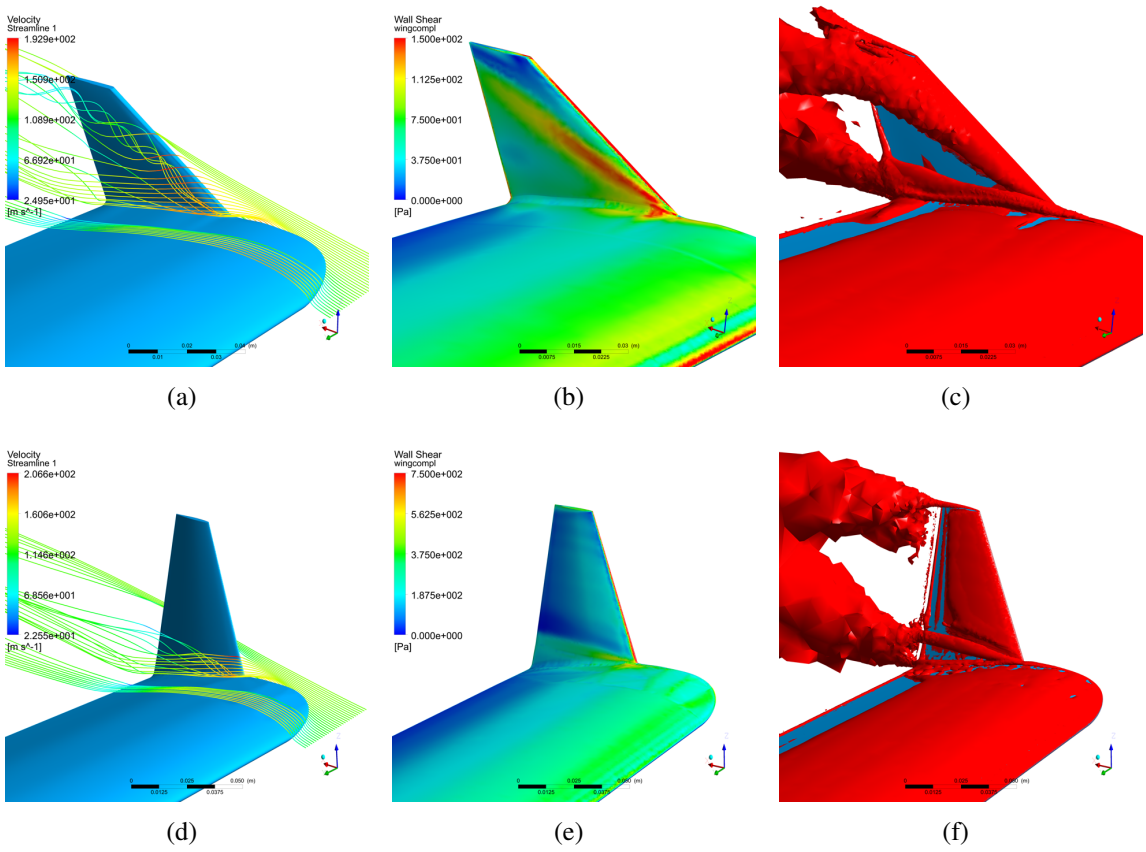

Figure 9: Vortex and wall shear comparison on the two winglets at $\alpha = 6°$ and zero sideslip. The new winglet is plotted at the flight Reynolds number to avoid stalling problems [1]. The limits for the pressure were scaled by a factor of 5 to result in comparable images.

Conclusion

This paper discussed the aerodynamic characteristics of a winglet design for a Fairchild Merlin III 8-seat, twin turboprop aircraft. The winglet originally tested was designed by the aircraft owner to improve the aesthetics of the aeroplane. To ensure that the winglet will not have any negative effect on the aircraft, a series of comparative CFD simulations was carried out. A hybrid mesh with unstructured surface- and volume grids, in addition to a structured boundary layer mesh was used on the wing, which was isolated from the fuselage.

Based on the findings for the original winglet, a new, improved design was tested. It featured less sweep and twice the surface area, with a NACA 64009 aerofoil. This new design improved the cruise L/D by 5%, which is a threefold improvement over the original winglet. At the same time, the skin friction drag was found to be similar, despite the large change in area. Finally, the wing bending moment was only increased by an additional 2% in cruise. The performance gains of the new winglet design were comparable to industry standards reported in literature.

References

[1] Kai Lehmkuehler. Winglet design for a fairchild merlin iii using cfd analysis. *Honours Thesis*, University of Sydney, 2010.

[2] Keisuke Asai. Theoretical considerations in the aerodynamic effectiveness of winglets. *JOURNAL OF AIRCRAFT*, 22(7), 1985.

[3] Richard T. Whitcomb. A design approach and selected wind-tunnel results at high subsonic speeds for wingtip mounted winglets. *NASA TN D-8260*, 1976.

[4] Bruce J. Holmes, Cornelis P. van Dam, Philip W. Brown Deal, and Perry L. Flight evaluation of the effect of winglets on performance and handling qualities of a single-engine general aviation airplane. *NASA Technical Memorandum 81892*, 1980.

[5] Timothy J. Baker. Mesh generation: Art or science? *Progress in Aerospace Sciences*, 41:29–63, 2005.

[6] Dimitri J. Mavriplis, John C. Vassberg, Edward N. Tinoco, Mori Mani, Olaf P. Brodersen, Bernhard Eisfeld, Richard A. Wahls, Joseph H. Morrison, Tom Zickuhr, David Levy, and Mitsuhiro Murayama. Grid quality and resolution issues from the drag prediction workshop series. *JOURNAL OF AIRCRAFT*, Vol. 46(3), 2009.

[7] Ansys. Ansys cfx 12 manuals, 2009. Available from: `CFXhelpfiles`.

[8] Elizabeth Lee-Rausch, Neal Frink, Dimitri Mavriplis, Russ Rausch, and William Milholen. Transonic drag prediction on a dlr-f6 transport configuration using unstructured grid solvers. *42nd AIAA Aerospace Sciences Meeting and Exhibit, Reno, Nevada*, AIAA-554, 2004.

[9] Martin Hepperle. Javafoil, 2007. Available from: `www.mh-aerotools.de/airfoils/javafoil.htm`.

[10] S. Hoerner. *Fluid-Dynamic Drag*. self published, 1965.

[11] Thomas Melin. *A Vortex Lattice MATLAB Implementation for Linear Aerodynamic Wing Applications*. PhD thesis, 2000.

[12] David C. Wilcox. *Turbulence Modeling for CFD*. DCW Industries, 2006.

[13] James L. Thomas, Boris Diskin, and Christopher L. Rumsey. Toward verification of unstructured-grid solvers. *JOURNAL OF AIRCRAFT*, Vol. 46, No. 12, 2008.

[14] F. R. Menter. Two-equation eddy-viscosity turbulence models for engineering applications. *AIAA JOURNAL*, 32(8), 1994.

[15] III Marchman, J. F., D. Manor, and H. F. Faery. Whitcomb winglet applications to general aviation aircraft. *AIAA, Aircraft Systemsand Technology Conference, Los Angeles, Calif.*, AIAA-1478, 1978.

[16] Cornells P. van Dam, Bruce J. Holmest, and Calvin Pitts. Effect of winglets on performance and handling qualities of general aviation aircraft. *JOURNAL OF AIRCRAFT*, VOL. 18, NO. 7, 1981.